

# Bond-orientational analysis of hard-disk and hard-sphere structures

V. Senthil Kumar and V. Kumaran<sup>a)</sup>*Department of Chemical Engineering, Indian Institute of Science, Bangalore 560 012, India*

(Received 23 January 2006; accepted 14 March 2006; published online 25 May 2006)

We report the bond-orientational analysis results for the thermodynamic, random, and homogeneously sheared inelastic structures of hard-disks and hard-spheres. The thermodynamic structures show a sharp rise in the order across the freezing transition. The random structures show the absence of crystallization. The homogeneously sheared structures get ordered at a packing fraction higher than the thermodynamic freezing packing fraction, due to the suppression of crystal nucleation. On shear ordering, strings of close-packed hard-disks in two dimensions and close-packed layers of hard-spheres in three dimensions, oriented along the velocity direction, slide past each other. Such a flow creates a considerable amount of fourfold order in two dimensions and body-centered-tetragonal (bct) structure in three dimensions. These transitions are the flow analogs of the martensitic transformations occurring in metals due to the stresses induced by a rapid quench. In hard-disk structures, using the bond-orientational analysis we show the presence of fourfold order. In sheared inelastic hard-sphere structures, even though the global bond-orientational analysis shows that the system is highly ordered, a third-order rotational invariant analysis shows that only about 40% of the spheres have face-centered-cubic (fcc) order, even in the dense and near-elastic limits, clearly indicating the coexistence of multiple crystalline orders. When layers of close-packed spheres slide past each other, in addition to the bct structure, the hexagonal-close-packed (hcp) structure is formed due to the random stacking faults. Using the Honeycutt-Andersen pair analysis and an analysis based on the 14-faceted polyhedra having six quadrilateral and eight hexagonal faces, we show the presence of bct and hcp signatures in shear ordered inelastic hard-spheres. Thus, our analysis shows that the dense sheared inelastic hard-spheres have a mixture of fcc, bct, and hcp structures. © 2006 American Institute of Physics. [DOI: 10.1063/1.2193150]

## I. INTRODUCTION

The Voronoi polyhedron of a nucleus point in space is the innermost polyhedron formed by the perpendicularly bisecting planes between the given nucleus and all the other nuclei.<sup>1</sup> The Voronoi tessellation divides a region into space-filling, nonoverlapping convex polyhedra. The salient properties of Voronoi tessellation are the following.

- Any point inside a Voronoi cell is closer to its nucleus than any other nuclei, Fig. 1. The Voronoi cells are space filling and hence a precise definition of local volume.<sup>2</sup>
- It gives a definition of geometric neighbors. The nuclei sharing a common Voronoi surface are geometric neighbors. Points on the shared surface are equidistant to the corresponding pair of nuclei. Hence geometric neighbors are competing centers in a growth scenario.
- Voronoi cells of hard-spheres are irregular at lower packing fractions but become regular as the regular close packing is approached. Thus, they are useful in characterizing all structures, from random to regular.

These properties qualify Voronoi tessellation as an important tool in the structural analysis of random media such as glass, packings, foams, cellular solids, proteins, etc.<sup>3-5</sup>

Voronoi tessellation occurs naturally in growth processes such as crystallization and plant cell growth, see Boots.<sup>6</sup> It is used (and was rediscovered under different names) in various fields such as meteorology, geology, ecology, metallography, archeology, etc. The statistical distributions of many Voronoi cell properties are reported, see Zhu *et al.*,<sup>7</sup> Oger *et al.*,<sup>8</sup> and the references therein. Our earlier works report the cell volume distributions and neighbor statistics for hard-particle structures.<sup>9-11</sup> In this work we do the bond-orientational analysis for thermodynamic, random, and sheared inelastic hard-disk and hard-sphere structures, with particular focus on the dense sheared microstructure.

We study three types of hard-particle structures: thermodynamic or canonical Monte Carlo (*NVE-MC*), the swelled random structures, and the sheared inelastic structures. The *NVE-MC* configurations are made with 50% success rate, i.e., the amplitude of the random trial displacement is continuously adjusted such that 50% of the trials lead to non-overlapping configurations. The swelled random structures are generated using a Monte Carlo adaptation of Woodcock's<sup>12</sup> algorithm: swell the nearest neighbors till they touch each other, give random trial displacements (with, say, 50% success rate as in *NVE-MC*) for all the particles, and continue the swelling and random displacement processes till the desired packing fraction is attained. Further details on the swelling algorithm are available in our earlier work.<sup>10</sup> In Sec. II we outline the Lees-Edwards boundary conditions,<sup>13,14</sup> us-

<sup>a)</sup>Electronic mail: kumaran@chemeng.iisc.ernet.in

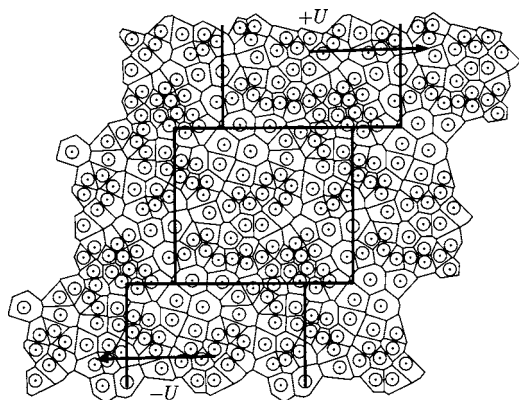


FIG. 1. A configuration with Lees-Edwards boundary conditions and Voronoi tessellation, with periodic boundary conditions (PBC).

ing which we generate the homogeneously sheared inelastic hard-disk and hard-sphere configurations. Every particle is said to be connected with its Voronoi neighbor by a *bond*. The orientation of these bonds is characterized by angular measures. The rotationally invariant functions defined on these angular measures are used in the bond-orientational analysis to describe the angular order of the local neighborhood.<sup>15,16</sup> This analysis is useful in characterizing the microstructures and quantifying the degree of local crystallization.

In Sec. III we present the global and local bond-orientational analysis of hard-disk structures. The sixfold and fourfold orders in the hard-disk systems are monitored at different packing fractions. The thermodynamic hard-disk structures have negligible fourfold order, and the sixfold order increases sharply across the freezing transition. The random hard-disk structures have a low global sixfold ordering, but there is a considerable amount of local crystallization, since the triangular structure maximizes both the local and global packing. In a homogeneous shear field, the crystal nucleation gets suppressed, as noted in the Brownian dynamics simulations of colloidal suspension by Butler and Harrowell,<sup>17</sup> Blaak *et al.*,<sup>18</sup> and our earlier granular simulations.<sup>11</sup> Due to the suppression of crystal nucleation, the sheared structures get ordered at a packing fraction higher than the thermodynamic freezing packing fraction. On shear ordering, strings of close-packed hard-disks, oriented along the velocity direction, slide past each other, creating considerable amount of fourfold order. This triangle-to-square symmetry change is the two-dimensional analog of the martensitic transformations observed in metals due to stresses induced by a rapid quench. While the transition in the metallic systems is due to diffusionless lattice distortions occurring at rates comparable to the speed of sound,<sup>19</sup> the transition in the flow systems is due to the sliding of close-packed layers past each other occurring over flow time scales.

In Sec. IV we present the bond-orientational analysis results for the hard-sphere systems. The global analysis shows the onset of order in thermodynamic structures across the freezing transition, the absence of order in random structures, and the suppression of nucleation in the homogeneously sheared structures. In sheared structures, even

though the global analysis shows considerable level of order, the local analysis using a third-order rotational invariant, devised by Mitus *et al.*,<sup>20</sup> shows that the fraction of spheres having face-centered-cubic (fcc) order is only about 40%, even in the dense and near-elastic limits. This clearly indicates the coexistence of multiple crystalline orders, which is explained as follows. On shear ordering, close-packed planes of spheres slide past each other, and spheres in a layer tend to occupy a position vertically above the centers of the spheres in the adjacent layers, forming bct structures. This fcc-to-bct transition is observed in the martensitic transformations exhibited by rapidly quenched metals. Also, when close-packed planes slide past each other, the random stacking faults form hexagonal-close-packed (hcp) structures. Using the Honeycutt-Andersen pair analysis<sup>21</sup> and an analysis based on the 14-faceted polyhedra having six quadrilateral and eight hexagonal faces, we show the presence of hcp and bct signatures in shear ordered inelastic hard-spheres. Thus, our analysis shows that the dense sheared inelastic hard-spheres have a mixture of fcc, hcp, and bct structures.

The diameter of a hard-disk or a hard-sphere is  $\sigma$ . The packing fraction of the system is  $\nu = (\pi/4)\sigma^2/v$  for hard-disks and  $\nu = (\pi/6)\sigma^3/v$  for hard-spheres, where  $v = V/N$  is the specific volume a system of  $N$  particles occupying a volume  $V$ .

## II. HOMOGENEOUSLY SHEARED INELASTIC HARD STRUCTURES

We use the Lees-Edwards boundary conditions<sup>13</sup> to generate homogeneously sheared inelastic hard-particle configurations, Fig. 1. The simulation box dimensions are  $l_x$ ,  $l_y$ , and  $l_z$ . In our simulation geometry,  $x$ ,  $y$ , and  $z$  are the velocity, gradient, and vorticity directions, respectively. In two-dimensional simulations, the  $z$  direction is absent. The top and the bottom boxes move with velocities  $+U$  and  $-U$ , respectively, with respect to the central box. When a particle crosses the top/bottom boundary of the central box with a horizontal velocity  $v_x$ , its image enters through the bottom/top with a horizontal velocity  $(v_x)_{\text{image}} = v_x \mp U$ . This induces shear at the top/bottom boundaries of the central box, which then propagates by collisions into the central box. The post-collisional velocity  $\mathbf{u}'$  of the smooth particles of identical mass undergoing a binary collision is given in terms of the precollisional velocities as

$$\mathbf{u}'_1 = \mathbf{u}_1 - \frac{1 + \epsilon}{2}(\mathbf{w} \cdot \mathbf{k})\mathbf{k},$$

$$\mathbf{u}'_2 = \mathbf{u}_2 + \frac{1 + \epsilon}{2}(\mathbf{w} \cdot \mathbf{k})\mathbf{k},$$

where  $\mathbf{w} = \mathbf{u}_1 - \mathbf{u}_2$ ,  $\mathbf{k}$  is the unit vector along the line joining the centers of the colliding particles 1 and 2, and  $\epsilon$  is the coefficient of normal restitution. In this work we use a constant coefficient of restitution model for the inelastic collisions. The energy input to the system due to shear is lost within the system by inelastic collisions; hence a thermostat is not required. When the system is below its shear ordering packing fraction, a linear velocity profile with a shear rate

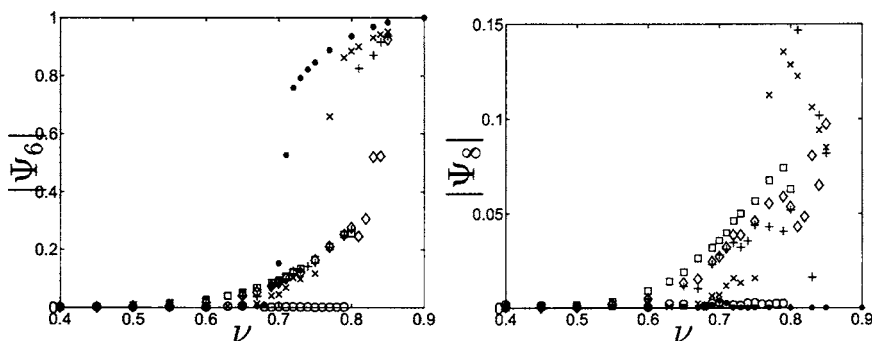


FIG. 2.  $|\Psi_6|$  and  $|\Psi_8|$  for hard-disks: thermodynamic structures ( $\bullet$ ), random structures ( $\circ$ ) generated at 90% success rate, and sheared inelastic structures at  $\epsilon=0.80$  ( $\square$ ),  $0.90$  ( $\diamond$ ),  $0.95$  ( $+$ ), and  $0.99$  ( $\times$ ). Thermodynamic and sheared structures data averaged for 10 000 configurations and random structures data averaged for 1000 configurations of 256 hard-disks, with PBC.

$\dot{\gamma}=U/l_y$  is induced in the central box. Above the shear ordering packing fraction, the close-packed layers slide over each other intermittently and a linear velocity profile does not develop, see for example, Fig. 10 of Ref. 22. Further details on the inelastic hard-particle implementation of the algorithm are available in Refs. 14 and 23. In our simulations the initial state is the hexagonal packing for hard-disks and fcc packing for hard-spheres. To disintegrate the initial lattice, we allow 100 elastic collisions per particle. Then the collisions are made inelastic, and the granular temperature is monitored. We found that allowing 5000 inelastic collisions per particle is sufficient to reach steady state. We have ensured that our structural statistics are unaffected by the initial lattice by using the swelled random<sup>9</sup> initial configurations.

### III. HARD-DISK STRUCTURES

The  $m$ -fold global bond-orientational order parameter<sup>15</sup> is defined as

$$\Psi_m = \langle \exp(im\theta) \rangle, \quad (1)$$

where  $\langle \cdot \rangle$  is the average over all the Voronoi neighbor bonds in the system and  $\theta$  is the angle formed by a bond with respect to some arbitrary axis. For a perfect  $m$ -fold ordered system,  $|\Psi_m|$  is unity and lower otherwise. To recognize the freezing of hard-disks into hexagonal-close-packed structure,  $|\Psi_6|$  is used.<sup>24</sup> Figure 2 shows the  $|\Psi_6|$  for thermodynamic, random, and sheared inelastic hard-disk structures, from which we observe the following.

- At the freezing packing fraction ( $\nu_F \approx 0.691$ , Ref. 25),  $|\Psi_6|$  for the thermodynamic hard-disk structure rises sharply due to the onset of hexagonal order. Above the melting packing fraction ( $\nu_M \approx 0.716$ , Ref. 25), the  $|\Psi_6|$  is close to unity indicating highly *correlated* local order.
- $|\Psi_6|$  for the dense random hard-disk structures is low, due to the absence of correlated order. In hard-disk packings, the structure maximizing the local and the global packing are identical, i.e., the triangular or the hexagonal structure. This lack of geometric frustration is considered to be the cause of the instability of dense random hard-disk packings against compressive forces.<sup>26,27</sup> (In three dimensions, the locally densest packing, viz., the tetrahedral packing is not space filling. This geometric frustration is considered to be the cause of the stability of dense random hard-sphere packings against compressive forces.) Thus, there is a considerable degree of local crystallization in dense

random hard-disk packings, shown below by the *local* bond-orientational analysis. However, the orientation of the local crystalline domains is uncorrelated. Hence,  $\Psi_6$  has a low value for the dense random hard-disk structures.

- Even for  $\epsilon=0.99$ , i.e., near-elastic limit, the sheared structures get ordered only above  $\nu \approx 0.77$ . The shear ordering packing fraction being higher than the thermodynamic freezing packing fraction shows the suppression of crystal nucleation by homogeneous shear. This phenomenon is also observed in the Brownian dynamics simulations of colloidal suspension by Butler and Harrowell<sup>17</sup> and Blaak *et al.*<sup>18</sup> and in our earlier granular simulations.<sup>11</sup>
- For  $\epsilon=0.99$ ,  $0.95$ , and  $0.90$ , the shear ordering packing fractions are  $\approx 0.77$ ,  $0.81$ , and  $0.83$ , respectively. This shows that as inelasticity increases shear ordering occurs at a higher packing fraction.

On shear ordering, strings of close-packed hard-disks, oriented in the velocity direction, slide past each other. This phenomenon was demonstrated in the shear of monolayers of polystyrene spheres suspended at the decane-water interface by Stancik *et al.*<sup>28</sup> When strings of close-packed hard-disks slide past each other, the distance between adjacent strings need to be greater than  $\sigma$ , at least locally, while the distance between adjacent strings is  $(\sqrt{3}/2)\sigma$  in the hexagonal-close-packed structure. When strings of close-packed hard-disks slide past each other, square or rhombic structures are

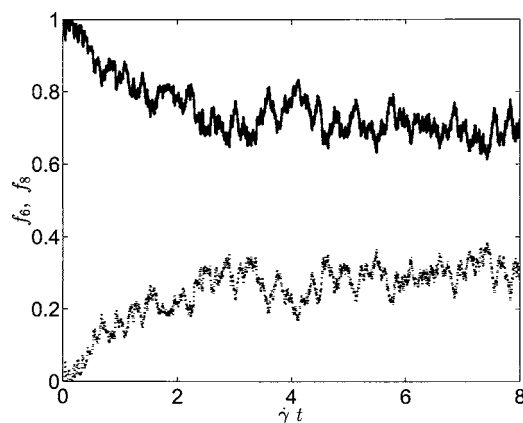


FIG. 3. Evolution of  $f_6$  (continuous line) and  $f_8$  (dotted line) in a sheared inelastic hard-disk simulation run at  $\nu=0.72$  and  $\epsilon=0.90$ . Initial configuration was the hexagonal lattice.

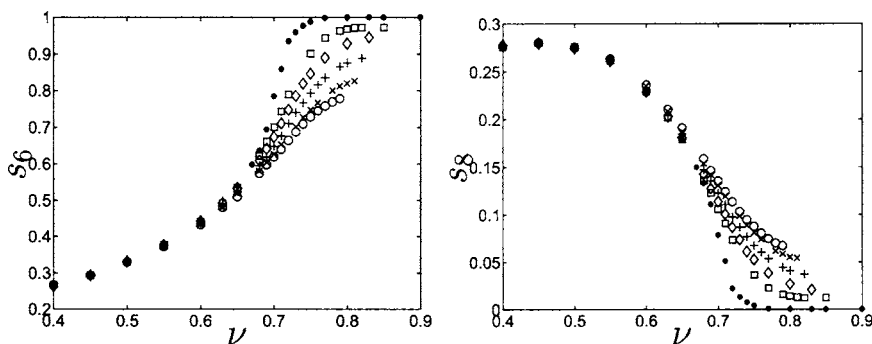


FIG. 4.  $s_6$  and  $s_8$  for hard-disks: thermodynamic structures ( $\bullet$ ) and random structures generated at success rates of 10% ( $\square$ ), 30% ( $\diamond$ ), 50% ( $+$ ), 70% ( $\times$ ), and 90% ( $\circ$ ). Averaging as in Fig. 2.

formed. Weiss *et al.*<sup>29</sup> have observed this triangle-to-square transition in the flow of confined monolayer colloidal suspensions and consider it the two-dimensional flow analog of martensitic transformations observed in metallic systems occurring due to the stresses induced by a rapid quench. Due to the topological instability of the square lattice to slight perturbations,  $|\Psi_8|$  is commonly used to monitor the distorted fourfold order instead of  $|\Psi_4|$ . The  $|\Psi_8|$  data for the thermodynamic, random, and sheared structures are given in Fig. 2, from which we observe the presence of a significant amount of fourfold order in the sheared hard-disk structures.

Next we proceed to the local analysis, using the method of Weiss *et al.*<sup>29</sup> The  $m$ -fold local bond-orientational order parameter of disk  $j$  with  $N_1$  Voronoi neighbors is

$$\psi_m = \frac{1}{N_1} \sum_{k=1}^{N_1} \exp(im\theta_k). \quad (2)$$

If  $|\psi_6| > |\psi_8|$  then a disk is said to have a sixfold coordination and fourfold coordination otherwise. The fractions of disks having sixfold and fourfold coordinations are  $f_6$  and  $f_8(=1-f_6)$ , respectively. When the homogeneous shear is switched on at time  $t=0$  in an equilibrated hard-disk configuration above its shear ordering packing fraction, due to the sliding of close-packed hard-disk strings, the sixfold coordination decreases and the fourfold coordination increases until the system reaches a steady state, Fig. 3. If the initial packing is disordered, even though the system packing fraction is above the shear ordering packing fraction, then the system initially gets ordered into layers, before the layers start sliding past each other. Then, during the initial ordering  $f_6$  increases, before it starts decreasing due to the sliding motion. The symmetry change involved in this triangle-to-square transition is analogous to the martensitic transformation ob-

served in metallic systems. However, the time scales involved are different. The martensitic transformation occurs by a *diffusionless* lattice distortion, at rates comparable to the speed of sound.<sup>19</sup> The transition observed in these dense flow systems are due to the formation, unlocking, and sliding of close-packed layers, which occurs over flow time scales.

A disk is considered to be *ordered*, if  $|\psi_6| > 0.5$  or  $|\psi_8| > 0.5$ . The fractions of ordered sixfold and fourfold disks are  $s_6$  and  $s_8$ , respectively. The  $s_6$  and  $s_8$  data for the thermodynamic and random structures are shown in Fig. 4, from which we observe the following.

- For  $\nu > \nu_F$ , most of the disks in the thermodynamic structure are sixfold ordered disks.
- For  $\nu < \nu_F$ , the random structures are identical with the thermodynamic structures, while they are distinct for  $\nu > \nu_F$ .
- In random hard-disk structures, due to the lack of geometric frustration, there is a significant amount of crystallites. However, this was not evident in the global analysis (Fig. 2) since the orientation of the local crystallites was uncorrelated.
- At lower success rates the fraction of crystallites ( $s_6$ ) is high, since the relatively large trial displacements tend to equilibrate the local nonequilibrium structures. At higher success rates, the trial displacements are small and the swelling process tends to lock the particles into random structures. These observations are reversed for the fraction of square defects ( $s_8$ ).

The  $s_6$  and  $s_8$  data for the thermodynamic and sheared structures are shown in Fig. 5, from which we observe the following.

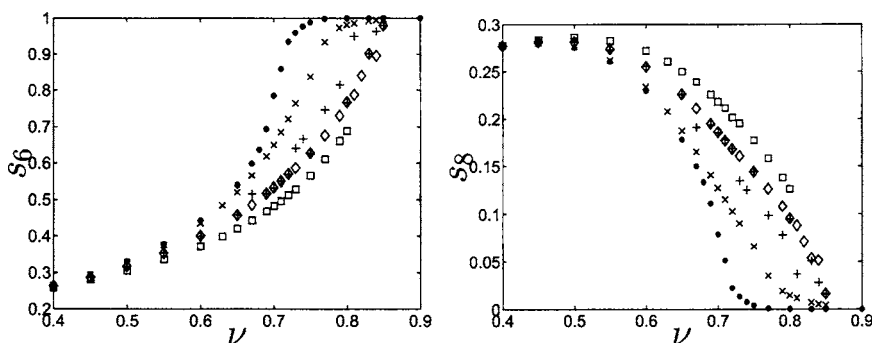


FIG. 5.  $s_6$  and  $s_8$  for hard-disks: thermodynamic structures ( $\bullet$ ) and sheared inelastic structures at  $\epsilon=0.80$  ( $\square$ ), 0.90 ( $\diamond$ ), 0.95 ( $+$ ), and 0.99 ( $\times$ ). Averaging as in Fig. 2.

TABLE I. System size dependence check for sheared inelastic hard-disk structure  $f_6$ ,  $s_6$  and  $s_8$ , for a constant coefficient of restitution  $\epsilon=0.99$ .

$\nu$	Run	$f_6$	$s_6$	$s_8$
0.60	I <sup>a</sup>	0.6015	0.4347	0.2333
	II <sup>b</sup>	0.6022	0.4359	0.2326
	III <sup>c</sup>	0.6019	0.4356	0.2331
	IV <sup>d</sup>	0.6034	0.4368	0.2324
0.70	I	0.7628	0.6497	0.1274
	II	0.7616	0.6488	0.1280
	III	0.7624	0.6499	0.1280
	IV	0.7624	0.6501	0.1278
0.75	I	0.8873	0.8375	0.0658
	II	0.8881	0.8385	0.0653
	III	0.8823	0.8284	0.0661
	IV	0.8869	0.8355	0.0643
0.80	I	0.9830	0.9808	0.0143
	II	0.9771	0.9716	0.0176
	III	0.9533	0.9346	0.0296
	IV	0.9518	0.9306	0.0273

<sup>a</sup>Averaged for 10 000 configurations of 256 hard-disks, with PBC.

<sup>b</sup>Averaged for 6400 configurations of 400 hard-disks, with PBC.

<sup>c</sup>Averaged for 2850 configurations of 900 hard-disks, with PBC.

<sup>d</sup>Averaged for 1600 configurations for 1600 hard-disks, with PBC.

- In dense sheared systems, due to the sliding of hard-disk strings past each other considerable concentration of square defects is generated in the systems. However, at higher densities they get compacted out due to the lack of geometric frustration, and the concentration of the crystallites tends towards unity.
- At a given packing fraction, as inelasticity increases, the concentration of the square defects ( $s_8$ ) increases, with a consequent decrease in the concentration of the crystallites ( $s_6$ ). This is the structural cause for the increase in shear ordering packing fraction with increasing inelasticity.

The system size dependence check for sheared hard-disk structures  $f_6$ ,  $s_6$ , and  $s_8$  are given in Table I. Note that there is negligible size dependence for packing fractions below the shear ordering packing fraction and nonsystematic size dependence for the packing fractions above it, due to the intermittent flow of close-packed hard-disk strings.

#### IV. HARD-SPHERE STRUCTURES

To every bond, formed between a sphere and its Voronoi neighbor, one can assign a spherical harmonic  $Y_{lm}(\theta, \phi)$ , where  $0 \leq \theta \leq \pi$  and  $0 \leq \phi < 2\pi$  are the angles made by the bond with respect to some reference frame. The actual value of  $Y_{lm}$  depends on the orientation of the reference frame; hence the second- and third-order rotationally invariant combinations are used in the bond-orientational analysis,<sup>16</sup>

$$Q_l = \left( \frac{4\pi}{2l+1} \sum_{m=-l}^l |Q_{lm}|^2 \right)^{1/2}, \quad (3)$$

where  $Q_{lm} = \langle Y_{lm} \rangle$  is the average over all the Voronoi bonds.  $Q_6$  is lowest order  $Q_l$  which gives a nonzero value for the

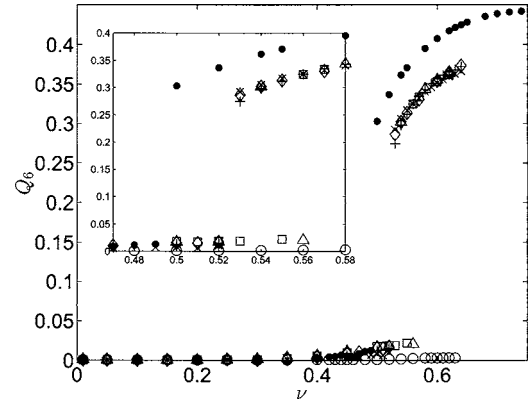


FIG. 6.  $Q_6$  for hard-spheres: thermodynamic structures ( $\bullet$ ), random structures ( $\circ$ ) generated at 50% success rate, and sheared inelastic structures at  $\epsilon=0.60$  ( $\triangle$ ),  $0.70$  ( $\square$ ),  $0.80$  ( $\diamond$ ),  $0.90$  ( $+$ ), and  $0.99$  ( $\times$ ). Thermodynamic and random structures data averaged for 1000 configurations of 256 hard-spheres, with PBC. Sheared structures data averaged for 675 configurations of 384 hard-spheres, with PBC.

common crystalline structures; hence, it is used as an order parameter to sense *any* kind of crystallization.<sup>16</sup> Richard *et al.*<sup>30</sup> have used  $Q_6$  to study the evolution of crystallization in the random hard-sphere packings. Figure 6 shows the  $Q_6$  data for thermodynamic, random, and sheared structures, from which we note the following.

- The freezing and melting packing fractions are, respectively,  $\nu_F \approx 0.494$  and  $\nu_M \approx 0.545$ .<sup>31</sup> The thermodynamic structures show a sharp rise in  $Q_6$  across the freezing transition. The dense random structures, due to the absence of crystallization, do not show a rise in  $Q_6$ .
- The suppression of crystal nucleation in a homogeneous shear field is evident in the  $Q_6$  data. While the thermodynamic ordering (i.e., the freezing) transition occurs at  $\nu_F \approx 0.494$ , the shear ordering transition occurs in the range of  $0.52$ – $0.53$  for  $\epsilon=0.80$ – $0.99$  and in the range of  $0.54$ – $0.55$  for  $\epsilon=0.70$  (details in the inset). Thus, the shear ordering packing fraction increases with increasing inelasticity.

For a local analysis, the local value of  $|Q_6|$  is not useful,

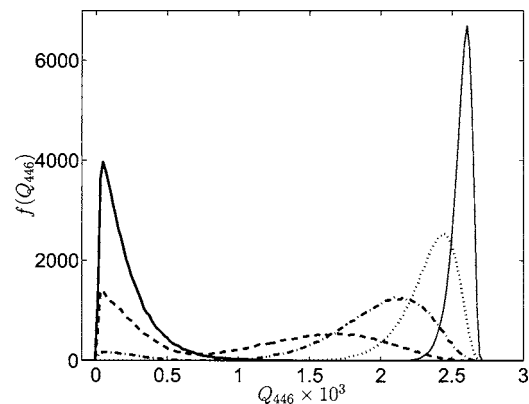


FIG. 7. Distribution of  $Q_{446}$  for hard-sphere thermodynamic structures at packing fractions  $\nu=0.49$  (thick line),  $0.50$  (---),  $0.55$  (-.-),  $0.60$  (···), and  $0.65$  (thin line).

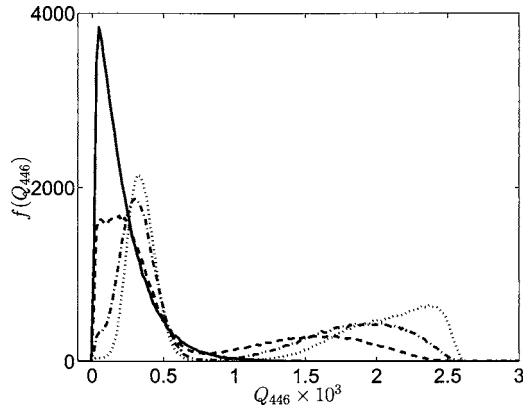


FIG. 8. Distribution of  $Q_{446}$  for sheared inelastic hard-spheres at a coefficient of restitution  $\epsilon=0.90$ , at packing fractions  $\nu=0.52$  (—),  $0.55$  (---),  $0.60$  (-.-), and  $0.64$  (···).

since it has a nonzero value for all the common crystalline structures. Hence, the third-order rotational invariant combinations are generally used,<sup>16</sup>

$$Q_{l_1 l_2 l_3} = \sum_{m_1+m_2+m_3=0} \begin{pmatrix} l_1 & l_2 & l_3 \\ m_1 & m_2 & m_3 \end{pmatrix} Q_{l_1 m_1} Q_{l_2 m_2} Q_{l_3 m_3}, \quad (4)$$

where  $(\cdot)$  are the Wigner  $3j$  symbols, the indices  $m_i = -l_i, \dots, l_i$  for  $i=1, 2, 3$ , and the summation is over the permutations satisfying the condition  $m_1+m_2+m_3=0$ . Mitus *et al.*<sup>20</sup> have shown that  $Q_{446}$ , defined on the 12 nearest neighbors (note the metric, non-Voronoi definition of neighbors), can be used to identify the local fcc structures. Gruhn and Monson<sup>32</sup> have used this method to monitor the fraction of fcc clusters formed during a hard-sphere solidification. With  $l_1=4$ ,  $l_2=4$ , and  $l_3=6$ , there are 75 terms in the summation of Eq. (4). An ideal fcc cluster has  $Q_{446} \approx 2.5 \times 10^{-3}$ . Figure 7 shows the  $Q_{446}$  distribution for the thermodynamic structures. The  $Q_{446}$  distribution has a two-peaked structure, which clearly distinguishes the fcc structures from the non-fcc structures. Mitus *et al.*<sup>20</sup> use the cutoff  $Q_{446}^c = 0.7 \times 10^{-3}$  to distinguish the fcc clusters from other local structures. This classification is not sensitive to the actual cutoff value, since the two peaks are well separated by a minimum. Figure 8 shows the  $Q_{446}$  distribution for the sheared system. We

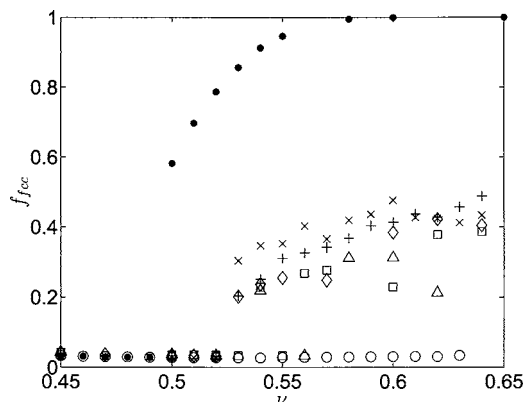


FIG. 9.  $f_{\text{fcc}}$  for hard-spheres: thermodynamic structures (●), random structures (○) generated at 50% success rate, and sheared inelastic structures at  $\epsilon=0.60$  (△),  $0.70$  (□),  $0.80$  (◇),  $0.90$  (+), and  $0.99$  (×). Averaging as in Fig. 6.

TABLE II. System size dependence check for sheared inelastic hard-sphere structure  $f_{\text{fcc}}$ , at  $\epsilon=0.99$ .

$\nu$	Run	$f_{\text{fcc}} \times 100$
0.45	I <sup>a</sup>	3.26
	II <sup>b</sup>	3.26
	III <sup>c</sup>	3.33
	IV <sup>d</sup>	3.31
0.50	I	2.87
	II	2.82
	III	2.93
	IV	2.96
0.55	I	40.47
	II	35.22
	III	46.52
	IV	41.61

<sup>a</sup>Averaged for 1200 configurations of 216 (six stacks of  $6 \times 6$ ) hard-spheres, with PBC.

<sup>b</sup>Averaged for 675 configurations of 384 (six stacks of  $8 \times 8$ ) hard-spheres, with PBC.

<sup>c</sup>Averaged for 450 configurations of 576 (nine stacks of  $8 \times 8$ ) hard-sphere, with PBC.

<sup>d</sup>Averaged for 288 configurations of 900 (nine stacks of  $10 \times 10$ ) hard-spheres, with PBC.

observe that shear does not affect the distinctness of the two peaks. Hence, the criterion  $Q_{446} > Q_{446}^c$  can be used to identify fcc clusters, even in the sheared configurations. The fraction of fcc clusters  $f_{\text{fcc}}$  so counted for the thermodynamic, random, and sheared structures are given in Fig. 9, from which we observe the following.

- The observations regarding the thermodynamic freezing transition, the lack of crystallization in random structures, and the suppression of crystal nucleation in the sheared structures are identical with those noted in the  $Q_6$  global analysis above.
- In the dense sheared structures, even in the dense and near-elastic limits, the fraction of fcc clusters is only about 40%. However, the global  $Q_6$  analysis in Fig. 6 showed that the sheared structures are considerably ordered. This is a clear indication of the coexistence of multiple crystalline structures (more below).

We show the size dependence check for  $f_{\text{fcc}}$  for the sheared structures in Table II. For packing fractions below the shear

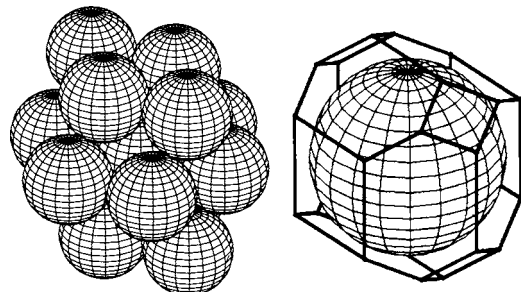


FIG. 10. An ideal bct cluster of 15 spheres (left) and the Voronoi polyhedron of the central sphere in the cluster (right). The figures share the same view but have different scales.

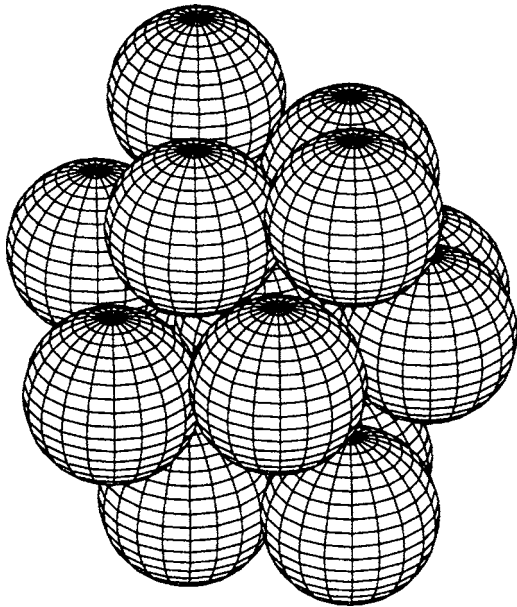


FIG. 11. A real bct cluster of 15 spheres formed during the homogeneous shear of inelastic hard-spheres having a coefficient of restitution  $\epsilon=0.90$ , at a packing fraction  $\nu=0.59$ .

ordering packing fraction, there is negligible size dependence. For packing fractions between shear ordering and the maximum shearable packing fraction  $\nu_m \approx 0.641$ ,<sup>33</sup> there is a mild but nonsystematic variation due to the intermittent sliding of close-packed layers past each other.

Before we proceed further with the microstructural analysis, we describe the body-centered-tetragonal structure. In the bct lattice, the lattice parameters are  $\{a, a, c\}$ , with  $c \neq a$  in general. With  $c=a$ , the bct lattice reduces to the body-centered-cubic (bcc) lattice. A bct cluster contains 15 spheres, with six spheres around the central sphere, forming a hexagonally close-packed plane, and four spheres on either sides, Fig. 10. The four spheres above and below the central layer are also close packed, but these spheres instead of occupying the tetrahedral voids offered by the central layer spheres (as in the close-packed fcc or hcp structures) are vertically above the midpoints of the central layer spheres. Hence, even though the layers are close packed, the stacking is not. In an ideal bct cluster, a central sphere has ten neighbors at a distance  $c=\sigma$  and four spheres at a distance  $a=\sqrt{3}/2\sigma$ , where  $\sigma$  is the hard-sphere diameter. The Voronoi polyhedron of the central sphere in such a cluster is shown in Fig. 10. It has six square faces (along the three orthogonal

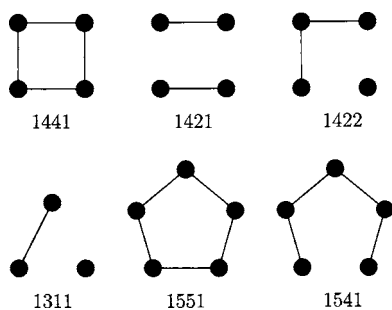


FIG. 12. Some of the bonds observed in dense particle systems.

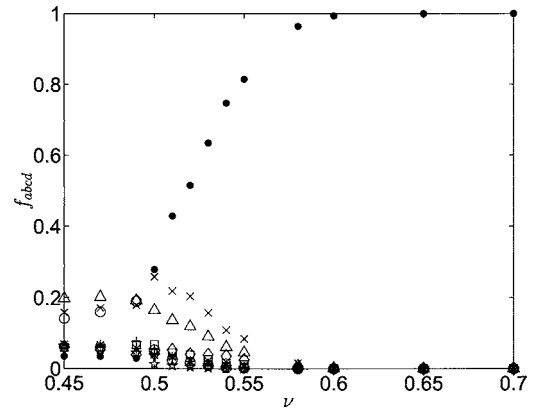


FIG. 13. Fraction of bonds of the type  $abcdef$  in thermodynamic hard-sphere structures.  $abcdef=1421$  (●), 1422 (\*), 1441 (□), 1661 (+), 1321 (★), 1551 (○), 1431 (△), 1541 (×), and 1311 (◇). Averaging as in Fig. 6.

axes) and eight hexagonal faces. Visualizing only the hexagon-forming spheres around the central sphere reveals the cuboidal view. In the cuboidal view, it is easily seen that the bct packing fraction is  $2\pi/9 \approx 0.6981$ . For further details on tetrahedral packing see O'Keefe<sup>34</sup> and the references therein.

On shear ordering, close-packed planes of spheres slide past each other in a zigzag path, with the close-packed planes oriented parallel to the velocity-vorticity plane. This phenomenon is observed in the plastic deformation of fcc crystals,<sup>35</sup> colloidal suspensions,<sup>36</sup> and in our earlier granular simulations.<sup>11</sup> When the close-packed layers slide thus past each other, the spheres in a layer tend to occupy a position vertically above the centers of the spheres in the adjacent layers. This leads to the formation of bct structures. Figure 11 shows a real bct cluster realized in our simulation, compare it with the ideal cluster in Fig. 10. This fcc-to-bct transition is the flow analog of the martensitic transformations observed in rapidly quenched metals. In addition to the bct structure, we can expect the *in situ* formation of hcp structure due to the following reason. The fcc and the hexagonal close packing (hcp) differ only in the stacking order, *ABC* and *ABA*, respectively. When close-packed planes slide past each other, the random stacking faults form hcp structures. This

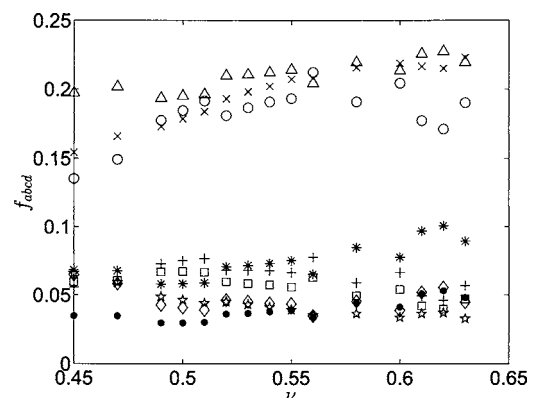


FIG. 14. Fraction of bonds of the type  $abcdef$  in swelled random hard-sphere structures, generated at 50% success rate.  $abcdef=1421$  (●), 1422 (\*), 1441 (□), 1661 (+), 1321 (★), 1551 (○), 1431 (△), 1541 (×), and 1311 (◇). Averaging as in Fig. 6.

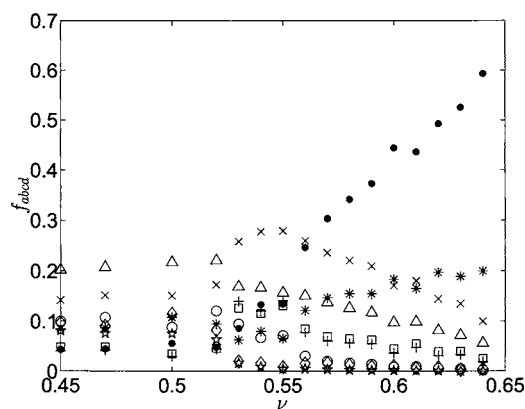


FIG. 15. Fraction of bonds of the type  $abcd$  in sheared inelastic hard-sphere structures, at a coefficient of restitution  $\epsilon=0.90$ .  $abcd=1421$  ( $\bullet$ ),  $1422$  ( $*$ ),  $1441$  ( $\square$ ),  $1661$  ( $+$ ),  $1321$  ( $\star$ ),  $1551$  ( $\circ$ ),  $1431$  ( $\triangle$ ),  $1541$  ( $\times$ ), and  $1311$  ( $\diamond$ ). Averaging as in Fig. 6.

phenomenon is observed in the shear of colloidal suspensions<sup>37</sup> and polymer solutions.<sup>38</sup> Gulley and Tao<sup>39</sup> have defined an order parameter to identify the formation of bct structure by electrorheological suspensions in the presence of an electric field. This order parameter is not useful for our system due to the coexistence of multiple crystalline structures. Hence we employ the Honeycutt-Andersen pair analysis,<sup>21</sup> which is widely used to study the microstructures in dense amorphous systems, such as metallic glasses (Duan *et al.*<sup>40</sup>), amorphous alloys (Pei *et al.*<sup>41</sup>), coating suspensions (Qi *et al.*<sup>42</sup>), etc.

In pair analysis, two particles are said to form a bond if the distance between them is less than a cutoff distance  $r_c$ . Particles forming a bond are said to be neighbors. Earlier applications of the pair analysis used a constant  $r_c$  (1.38 for fcc and hcp lattices and 1.54 for bcc lattice, in reduced units). However, Yu *et al.*<sup>43</sup> suggest the first minimum in the radial distribution function for fcc and hcp lattices and the second minimum for bcc lattices. In this work we take the first minimum in the radial distribution function as  $r_c$ . For sheared structures, we consider the angular averaged radial distribution function. Some of the bonds occurring in dense particle systems are illustrated in Fig. 12. Each pair of particles is characterized by four indices  $abcd$ . If two particles form a bond  $a=1$ , otherwise  $a=2$ . The number of neighbors common to a given pair of particles is  $b$ . The number of bonds among the common neighbors is  $c$ . The last index  $d$  is used

TABLE III. System size dependence for the fraction of bond types in sheared inelastic hard-disk structures at  $\nu=0.57$  and  $\epsilon=0.90$ .

$abcd$	I <sup>a</sup>	II <sup>b</sup>	III <sup>c</sup>	IV <sup>d</sup>
1421	0.3194	0.3036	0.3098	0.2862
1422	0.1392	0.1463	0.1287	0.1244
1441	0.0695	0.0693	0.0690	0.0696
1661	0.0598	0.0601	0.0598	0.0610
1321	0.0028	0.0035	0.0052	0.0093
1551	0.0184	0.0197	0.0189	0.0198
1431	0.1347	0.1374	0.1407	0.1476
1541	0.2347	0.2360	0.2352	0.2343
1311	0.0142	0.0157	0.0213	0.0309
others	0.0074	0.0084	0.0114	0.0618

<sup>a</sup>Averaged for 1200 configurations of 216 (six stacks of  $6\times 6$ ) hard-spheres, with PBC.

<sup>b</sup>Averaged for 675 configurations of 384 (six stacks of  $8\times 8$ ) hard-spheres, with PBC.

<sup>c</sup>Averaged for 450 configurations of 576 (nine stacks of  $8\times 8$ ) hard-spheres, with PBC.

<sup>d</sup>Averaged for 288 configurations of 900 (nine stacks of  $10\times 10$ ) hard-spheres, with PBC.

to distinguish structures which share the same value for the first three indices, especially to distinguish the 1421 and 1422 bonds. The general guidelines used to interpret the bonds are the following (Lee *et al.*<sup>44</sup>). fcc structure has only 1421 bonds, hcp structure has equal amounts of 1421 and 1422 bonds, bcc structure has 43% 1441 and 57% 1661 bonds, simple icosahedral structure has 71% 1321 and 29% 1551 bonds, large icosahedral structures have significant amounts of 1311 and 1422 bonds, with a decrease in 1321 and 1551 bonds, and 1431 and 1541 bonds are considered defective fcc and icosahedral structures, see Pei *et al.*<sup>41</sup>

The pair-analysis results for the thermodynamic structures are given in Fig. 13. A sharp rise in the 1421 bonds marks the onset of fcc order in hard-sphere solid phase. For  $\nu > \nu_F$ , the 1421 bonds increase at the expense of the defective fcc and icosahedral structures, i.e., 1431 and 1541 bonds. The pair-analysis results for the random structures are given in Fig. 14. The incidence of 1421 bonds and hence the formation of fcc crystallites are negligible. The dominant structures are the icosahedra (1551) and the defective structures (1541 and 1431). We are not aware of any work using pair analysis to analyze the presence of bct structures. The closest to the current work is that by Qi *et al.*,<sup>42</sup> which shows

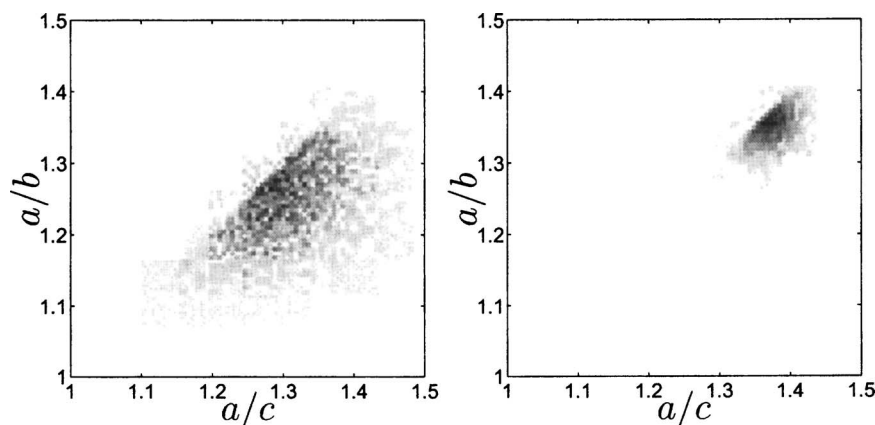


FIG. 16. The joint distribution of the ratios  $a/b$  and  $a/c$  at  $\nu=0.55$  (left) and  $\nu=0.65$  (right), for fcc hard-sphere solid structures. Darker region indicates higher probability.

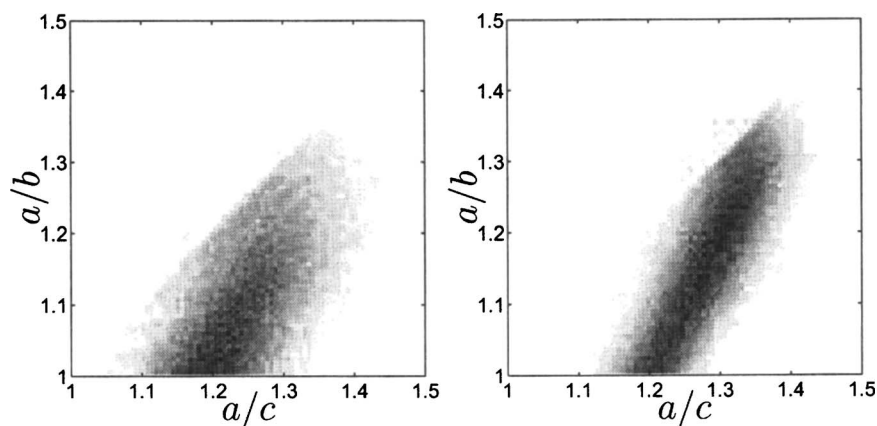


FIG. 17. The joint distribution of the ratios  $a/b$  and  $a/c$  at  $\nu=0.59$  (left) and  $\nu=0.64$  (right), for sheared inelastic hard-sphere structures at  $\epsilon=0.90$ .

the coexistence of fcc, hcp, and bcc structures, along with icosahedral disorder, in sheared coating suspensions. Hence, we have evolved the following additional rules by visually inspecting the local structures: good bct clusters (as in Fig. 11) have nearly equal amounts of 1421 and 1422 and distorted bct clusters have higher amounts of 1421, 1431, and 1541 bonds.

These two observations can be supported as follows: Jakse *et al.*<sup>45</sup> consider the bonds 1441, 1431, 1421, and 1422 to indicate local tetrahedral order. This supports the first observation. The dense amorphous structures, represented by icosahedral structures containing 1551 and 1541 bonds, have local tetrahedral order, since it maximizes the local packing. This supports the second observation. As mentioned earlier, when close-packed planes slide past each other, apart from bct structures, the hcp structures are also formed. Hence, we consider a preponderance of 1421 and 1422 bonds as a signature of *both* bct and hcp structures and not exclusively bct structure. The pair-analysis results for the sheared structures are given in Fig. 15. Using the above additional rules, we interpret the results as follows: in the high-dense limit, the sheared structures have about 60% 1421 and 20% 1422 bonds. Assuming that the bct+hcp structures are represented by equal amounts of 1421 and 1422 bonds, this implies that the fcc structure incidence is about 40%. This estimate tallies with our earlier local analysis in Fig. 9. There is about 10% of 1541 bonds and 8% of 1431, which could be defective bct structures. Note that the incidence of bcc bonds (1441 and 1661) is only about 6%. In a bct structure with  $c \neq a$ , the bcc-like bonds get counted as 1421 bonds and not as 1441

bonds. The size dependence check for the sheared structure pair analysis is given in Table III. There is a mild size dependence ( $<3\%$ ): With increasing system size the fcc bonds (1421) decreases, with an increase in icosahedral defects (1321 and 1311) and fcc defects (1431). However, this trend does not counter our conclusion that bct+hcp structures are coexisting with fcc structures. For packing fractions below the shear ordering packing fraction, the system size dependence is negligible.

Now we present an analysis based on the bcc-like polyhedra. Among the 14-faceted polyhedra, consider the particular case of the polyhedra having six quadrilateral and eight hexagonal faces. We call these polyhedra as the signature polyhedra, since they are useful in identifying the local lattice parameters (shown below). The neighbors of the signature polyhedron which form the six quadrilateral faces are nearly mutually orthogonal (shown in the Appendix). Hence, the local or *pseudolattice* parameters can be easily inferred from the distance between these neighbors and the central sphere. Note that these pseudolattice parameters are the actual lattice parameters only for bcc and bct structures (shown below). In a bcc solid phase most of the polyhedra are of this type. But in other solid structures, their incidence is about 10%–20%. We compute the local lattice parameters of the signature polyhedra as  $\{a, b, c\}$ , with  $a \geq b \geq c$ . We form the lattice ratios  $a/b$  and  $a/c$  and study their joint distribution. In the bcc lattice, both these ratios are unity. In the fcc lattice, due to a topological instability, some of the second neighbors get promoted as first neighbors and form small quadrilateral

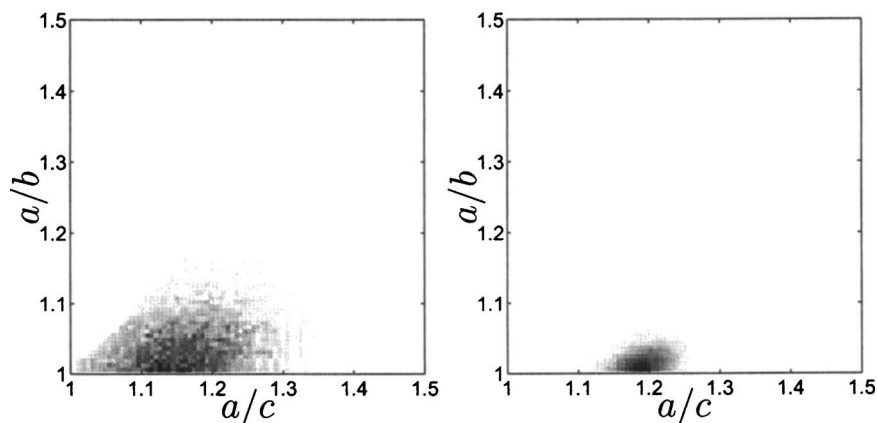


FIG. 18. The joint distribution of the ratios  $a/b$  and  $a/c$  at  $\nu=0.55$  (left) and  $\nu=0.65$  (right), for hcp hard-sphere solid structures.

TABLE IV. Percentage distribution of the number of faces of the Voronoi polyhedra for different structured systems at  $\nu=0.59$ .

$n$	$P_n \times 100$			
	bcc <sup>a</sup>	hcp <sup>b</sup>	fcc <sup>c</sup>	Sheared <sup>d</sup>
12	0.01	4.03	3.44	0.68
13	1.89	23.65	23.44	15.96
14	93.95	40.76	41.83	63.56
15	4.07	25.07	25.66	17.80
16	0.07	5.95	5.28	1.93
17	0	0.51	0.35	0.07
18	0	0.01	0.01	0

<sup>a</sup>Averaged for 100 configurations of 432 hard-spheres, with PBC.

<sup>b</sup>Averaged for 1000 configurations of 384 (six stacks of  $8 \times 8$ ) hard-spheres, with PBC.

<sup>c</sup>Averaged for 1000 configurations of 256 hard-spheres with PBC.

<sup>d</sup> $\epsilon=0.90$ , averaged for 675 configurations of 384 hard-spheres, with PBC.

face, described in our earlier work.<sup>9</sup> Such clusters form the 14-faceted polyhedra with  $a/b=a/c=\sqrt{2}$ . Note that the actual fcc lattice parameters are  $a=b=c$ . From Fig. 16, we observe that the thermodynamic fcc solid phase evolves along the diagonal  $a/b=a/c$  and approaches the value of  $\sqrt{2}$  in the regular close-packed limit. In the sheared structures, the signature polyhedra reveal the bct structure with the ratios  $a/b=1$  and  $a/c=\sqrt{3}/2 \approx 1.22$ . In Fig. 17, at  $\nu=0.59$  we observe that the joint distribution is centered around the bct values for a shear ordered system. However, near the maximum shearable packing fraction  $\nu_m \approx 0.641$ ,<sup>33</sup> the peak position of the joint distribution gets smeared towards the fcc value  $a/b=a/c=\sqrt{2}$ , since the nonshearing plug retains the fcc structure. Thus, this polyhedron analysis shows the bct signature in dense sheared systems. But it shares a shortcoming with the pair analysis that the bct and hcp structures respond identically. From Fig. 18, we note that the hcp solid also has  $a/b=1$  and  $a/c=\sqrt{3}/2$ . The bcc-like signature of the bct structure is found in the distribution of the number of faces ( $P_n$ ) of the Voronoi polyhedra, as shown in Table IV. The fcc and hcp structures have polyhedra with the number of faces in the range of 12–18, due to the topological instability, and share a nearly similarly distribution of faces. In

bcc structures the 14-faceted polyhedra are predominant. The predominance of the 14-faceted polyhedra in the dense sheared inelastic structures shows the bcc-like signature of the bct structure. Additionally a visual inspection, as in Fig. 11, confirms the bct signature in dense sheared inelastic hard-sphere structures.

## V. CONCLUSIONS

We report the bond-orientational analysis results for the thermodynamic, random, and homogeneously sheared inelastic structures of hard-disks and hard-spheres. The sixfold and fourfold orders in the hard-disk structures are monitored at different packing fractions. The thermodynamic structures contain negligible amount of fourfold order, and the sixfold order increases sharply across the freezing transition. The random hard-disk structures have low global sixfold order, yet considerable local crystallization is observed due to the lack of geometric frustration in two-dimensional systems. The local crystallization in the hard-disk random structures decreases with a decrease in the amplitude of the trial displacements involved in their generation. Due to the suppression of crystal nucleation, the sheared structures get ordered at a packing fraction higher than the thermodynamic freezing packing fraction. On shear ordering, strings of close-packed hard-disks, oriented along the velocity direction, slide past each other. When close-packed strings of disks slide past each other, considerable amount of fourfold order is created in the system. This triangle-to-square transition is the two-dimensional flow analog of the martensitic transformations occurring in metals due to the stresses induced by a rapid quench. While the transition in the metallic systems is due to diffusionless lattice distortions occurring at rates comparable to the speed of sound, the transition in the flow systems are due to the sliding of close-packed layers past each other occurring over longer time scales.

In the hard-sphere structures, the global bond-orientational analysis shows the onset of order in thermodynamic structures across the freezing transition, the absence of order in random structures, and the suppression of nucleation in the homogeneously sheared structures. In sheared structures, even though the global analysis shows a considerable

TABLE V. Percentage incidence and the orthogonality of the signature polyhedra in thermodynamic and sheared inelastic hard-sphere structures.

Type	$\nu$	Percentage incidence	$\mathcal{R}$		
			Minimum	Average	Maximum
Thermodynamic <sup>a</sup>	0.50	8.45	$6.9 \times 10^{-4}$	0.19	1.12
	0.60	8.77	$2.1 \times 10^{-4}$	0.05	0.27
	0.65	9.05	$8.0 \times 10^{-5}$	0.02	0.12
	0.70	9.23	$2.8 \times 10^{-5}$	0.003	0.02
Sheared <sup>b</sup>	0.55	7.61	$1.9 \times 10^{-4}$	0.14	1.32
	0.59	13.95	$5.3 \times 10^{-5}$	0.08	1.06
	0.61	16.99	$4.8 \times 10^{-5}$	0.07	0.94
	0.64	20.59	$1.2 \times 10^{-5}$	0.05	0.63

<sup>a</sup>Averaged for 1000 configurations of 256 hard-spheres, with PBC.

<sup>b</sup>Averaged for 675 configurations of 384 (six stacks of  $8 \times 8$ ) hard-spheres, with PBC and  $\epsilon=0.90$ .

level of order, a local analysis using a third-order rotational invariant, devised by Mitus *et al.*,<sup>20</sup> shows that the fraction of spheres having face-centered-cubic (fcc) order is only about 40%, even in the dense and near-elastic limits. Thus, the local analysis shows the presence of multiple crystalline structures in the system. On shear ordering, close-packed planes of spheres slide past each other in a zigzag path, with the close-packed planes oriented parallel to the velocity-vorticity plane. When the close-packed layers slide thus past each other, the spheres in a layer occupy a position vertically above the centers of the spheres in the adjacent layers, forming the body-centered-tetragonal (bct) structures. This fcc-to-bct transition is the flow analog of the martensitic transformations exhibited by rapidly quenched metals. Also, when close-packed planes slide past each other, the random stacking faults form hexagonal-close-packed (hcp) structures. Using the Honeycutt-Andersen pair analysis<sup>21</sup> and an analysis based on the 14-faceted polyhedra having six quadrilateral and eight hexagonal faces, we show the presence of bct and hcp signatures in shear ordered inelastic hard-spheres. Thus, our analysis shows that the dense sheared inelastic hard-spheres have a mixture of fcc, bct, and hcp structures.

#### APPENDIX: ORTHOGONALITY OF THE QUADRILATERAL FACES OF THE SIGNATURE POLYHEDRA

A fraction of the 14-faceted polyhedra have six quadrilateral and eight hexagonal faces. We call these bcc-like polyhedra as the *signature* polyhedra, since it is easy to deduce the local lattice parameters, as shown in Sec. IV. The near orthogonality of the neighbors contributing the quadrilateral faces is crucial to the quick estimation of the local lattice parameters, and we demonstrate it here. Let  $\mathbf{r}_i$ ,  $i = 1, \dots, 6$ , be the unit vectors along the lines joining the central sphere and the neighbors contributing the quadrilateral faces. We define the nonorthogonality factor as

$$\mathcal{R} = \sum_{i=1}^6 \sum_{j=1}^6 \mathbf{r}_i \cdot \mathbf{r}_j. \quad (\text{A1})$$

This quantity is zero if the  $r_i$  are mutually orthogonal. Because for any  $i$ , the contribution  $\mathbf{r}_i \cdot \mathbf{r}_i = 1$  gets canceled by the contribution  $\mathbf{r}_i \cdot \mathbf{r}_j = -1$ , where  $\mathbf{r}_j$  is the antiparallel of  $\mathbf{r}_i$ , and the four remaining unit vectors lying in the plane perpendicular to  $\mathbf{r}_i$  and  $\mathbf{r}_j$  make zero contributions. The outer summation in the definition of  $\mathcal{R}$  is necessary to locate the non-orthogonality among the unit vectors lying in the plane normal to a given pair of unit vector and its antiparallel. For slight distortions of an orthogonal set  $\{\mathbf{r}_i\}$ ,  $\mathcal{R}$  has a small nonzero value. Hence,  $\mathcal{R}$  is a measure of the nonorthogonality of the set  $\{\mathbf{r}_i\}$ . From Table V we observe that the range over which  $\mathcal{R}$  is distributed in the shear ordered structures is comparable with that in the thermodynamic structures at  $\nu = 0.50$ , which is just above the freezing transition  $\nu_F \approx 0.494$ . Hence, the signature polyhedra of the sheared structures are no more nonorthogonal than the just-frozen thermodynamic structures, in which the fcc order has set in. Hence, we consider that the six neighbors forming the quadrilateral

faces in any signature polyhedra to be nearly mutually orthogonal. Now, we separate the six neighbors contributing the quadrilateral faces into three pairs of which lie along the same direction, i.e., the neighbor having a unit vector  $\mathbf{r}_i$  and the neighbor having  $\mathbf{r}_j \cdot \mathbf{r}_i \approx -1$ . Half the distance between such a pair of spheres give the lattice parameter along that direction.

- <sup>1</sup>G. Voronoi, *J. Reine Angew. Math.* **134**, 198 (1908).
- <sup>2</sup>D. C. Rapaport, *Mol. Phys.* **48**, 23 (1983).
- <sup>3</sup>F. Aurenhammer, *ACM Comput. Surv.* **23**, 345 (1991).
- <sup>4</sup>A. Okabe, B. Boots, and K. Sugihara, *Spatial Tessellations: Concepts and Applications of Voronoi Diagrams* (Wiley, New York, 1992).
- <sup>5</sup>G. Schliecker, *Adv. Phys.* **51**, 1319 (2002).
- <sup>6</sup>B. N. Boots, *Metallography* **15**, 53 (1982).
- <sup>7</sup>H. X. Zhu, S. M. Thorpe, and A. H. Windle, *Philos. Mag. A* **81**, 2765 (2001).
- <sup>8</sup>L. Oger, A. Gervois, J. P. Trodec, and N. Rivier, *Philos. Mag. B* **74**, 177 (1996).
- <sup>9</sup>V. S. Kumar and V. Kumaran, *J. Chem. Phys.* **123**, 074502 (2005).
- <sup>10</sup>V. S. Kumar and V. Kumaran, *J. Chem. Phys.* **123**, 114501 (2005).
- <sup>11</sup>V. S. Kumar and V. Kumaran, *Phys. Rev. E* (to be published).
- <sup>12</sup>L. V. Woodcock, *J. Chem. Soc., Faraday Trans. 2* **72**, 1667 (1976).
- <sup>13</sup>A. W. Lees and S. F. Edwards, *J. Phys. C* **5**, 1921 (1972).
- <sup>14</sup>C. S. Campbell, *J. Fluid Mech.* **203**, 449 (1989).
- <sup>15</sup>B. I. Halperin and D. R. Nelson, *Phys. Rev. Lett.* **41**, 121 (1978).
- <sup>16</sup>P. J. Steinhardt, D. R. Nelson, and M. Ronchetti, *Phys. Rev. B* **28**, 784 (1983).
- <sup>17</sup>S. Butler and P. Harrowell, *Phys. Rev. E* **52**, 6424 (1995).
- <sup>18</sup>R. Blaak, S. Auer, D. Frenkel, and H. Lowen, *Phys. Rev. Lett.* **93**, 068303 (2004).
- <sup>19</sup>W. D. Callister, Jr., *Materials Science and Engineering. An Introduction*, 5th ed. (Wiley, New York, 2000).
- <sup>20</sup>A. C. Mitus, F. Smolej, H. Hahn, and A. Z. Patashinski, *Europhys. Lett.* **32**, 777 (1995).
- <sup>21</sup>J. D. Honeycutt and H. C. Andersen, *J. Phys. Chem.* **91**, 4950 (1987).
- <sup>22</sup>M. J. Stevens and M. O. Robbins, *Phys. Rev. E* **48**, 3778 (1993).
- <sup>23</sup>I. Goldhirsch and M. L. Tan, *Phys. Fluids* **8**, 1752 (1996).
- <sup>24</sup>G. F. Mazenko, *Equilibrium Statistical Mechanics* (Wiley-VCH, Berlin, 2000).
- <sup>25</sup>B. J. Alder and T. E. Wainwright, *Phys. Rev.* **127**, 359 (1962).
- <sup>26</sup>T. I. Quickenden and G. K. Tan, *J. Colloid Interface Sci.* **48**, 382 (1974).
- <sup>27</sup>E. L. Hinrichsen, J. Feder, and T. Jossang, *Phys. Rev. A* **41**, 4199 (1990).
- <sup>28</sup>E. J. Stancik, G. T. Gavranovic, M. J. O. Widenbrant, A. T. Laschitsch, J. Vermant, and G. G. Fuller, *Faraday Discuss.* **123**, 145 (2003).
- <sup>29</sup>J. A. Weiss, D. W. Oxtoby, and D. G. Grier, *J. Chem. Phys.* **103**, 1180 (1995).
- <sup>30</sup>P. Richard, L. Oger, J. P. Trodec, and A. Gervois, *Phys. Rev. E* **60**, 4551 (1999).
- <sup>31</sup>W. G. Hoover and F. H. Ree, *J. Chem. Phys.* **49**, 3609 (1968).
- <sup>32</sup>T. Gruhn and P. A. Monson, *Phys. Rev. E* **64**, 061703 (2001).
- <sup>33</sup>C. K. K. Lun and S. B. Savage, *Acta Mech.* **63**, 15 (1986).
- <sup>34</sup>M. O'Keeffe, *Acta Crystallogr., Sect. A* **54**, 320 (1998).
- <sup>35</sup>A. H. Cottrell, *Dislocations and Plastic Flow in Crystals* (Clarendon, Oxford, 1953).
- <sup>36</sup>B. J. Ackerson, *J. Rheol.* **34**, 553 (1990).
- <sup>37</sup>W. Loose and B. J. Ackerson, *J. Chem. Phys.* **101**, 7211 (1994).
- <sup>38</sup>J. Bang and T. P. Lodge, *J. Phys. Chem. B* **107**, 12071 (2003).
- <sup>39</sup>G. L. Gullety and R. Tao, *Phys. Rev. E* **56**, 4328 (1997).
- <sup>40</sup>G. Duan, D. Xu, Q. Zhang, G. Zhang, T. Cagin, W. L. Johnson, and W. A. Goddard III, *Phys. Rev. B* **71**, 224208 (2005).
- <sup>41</sup>Q. X. Pei, C. Lu, and H. P. Lee, *J. Phys.: Condens. Matter* **17**, 1493 (2005).
- <sup>42</sup>D. Qi, M. Joyce, and D. Fleming, *Powder Technol.* **104**, 50 (1999).
- <sup>43</sup>D. Q. Yu, M. Chen, and X. J. Han, *Phys. Rev. E* **72**, 051202 (2005).
- <sup>44</sup>H. J. Lee, T. Cagin, W. L. Johnson, and W. A. Goddard III, *J. Chem. Phys.* **119**, 9858 (2003).
- <sup>45</sup>N. Jakse, O. Lebacqz, and A. Pasturel, *Phys. Rev. Lett.* **93**, 207801 (2004).